THE ASTROPHYSICAL JOURNAL, 368:641–651, 1991 February 20

COLLISIONAL EXCITATION AND RADIATIVE PROPERTIES OF N II: THE STRONG INTERCOMBINATION (^1D–$^3P^o$) TRANSITION AT 748 Å

T. M. TRIPP AND D. E. SHEMANSKY
Lunar and Planetary Laboratory, University of Arizona, Tucson, AZ 85721
AND
G. K. JAMES AND J. M. AJELLO
Jet Propulsion Laboratory, Pasadena, CA 91109
Received 1990 April 9; accepted 1990 August 14

ABSTRACT

We have constructed a collisional radiative model, using a combination of theoretical calculations and experimental measurements, in order to calculate the excitation and emission properties of electron impact on N II. We have also conducted a spectrometric experiment in order to verify theoretical calculations predicting strong configuration interaction effects, and we find that the measured strength of the N II intercombination transition $2s^22p^2\ ^1D$–$2s^22p(^2P)3s\ ^3P^o$ at 748.37 Å is comparable to the electric dipole multiplet $2s^22p^2\ ^3P$–$2s^22p(^2P)3s\ ^3P^o$ at 671 Å. The measured branching ratio for the ^1D–$^3P^o$ ($J = 1$) transition is 0.29 ± 0.15, in agreement with recent theoretical calculations by Fawcett. Beam foil lifetime measurements for the $3s\ ^3P^o$ state are also in agreement with the theoretical calculations. This is a remarkably strong intercombination transition for such a light element. If enough strong intercombination transitions of this type exist in the carbon isoelectronic sequence, diagnostic data and collisional radiative quantities could be affected with important astrophysical ramifications. We have employed this finding and our model in a preliminary calculation N II radiative cooling and rate coefficients, and we have examined how the N II temperature diagnostic lines might be affected by intercombination cascading. In respect to planetary atmospheres research, we briefly discuss the excitation and radiative properties of N II excited directly by electrons and by electron dissociative ionization excitation of N_2.

Subject headings: atomic processes — transition rates — ultraviolet: spectra

1. INTRODUCTION

This paper presents an electronic structure model, constructed from a combination of theoretical and experimental data, which we have used to examine the excitation and radiative properties of N II. We also report experimental measurements of dissociative ionization excitation of N_2 by electrons in the EUV showing the strong intercombination transition at 748.37 Å. These measurements provide cross sections for N II emissions in the 670–750 Å range. The emission properties are discussed in the context of application to astrophysical diagnostics and the upper atmospheres of the Earth and Titan.

Detailed calculations of transition probabilities (Czyzak & Poirier 1985, and references therein) and collision strengths (Seaton 1975; Robb 1975; Saraph & Seaton 1974; Jackson 1973) that include configuration interaction have been made for N II spin-changing lines, but only for astrophysically important visible transitions between the ground state ($2s^22p^2\ 3P$), the lowest singlet states ($2s^22p^2\ ^1D$ and $2s^22p^2\ ^1S$), and the lowest quintet state ($2s2p^3\ ^5S^o$). These transitions are generally quite weak. Recently, however, Fawcett (1987, hereafter F87) has calculated oscillator strengths of ultraviolet N II transitions with a Hartree-Fock relativistic method that accounts for configuration interaction up to $n = 5$ and uses Slater parameter adjustment to account for other weakly interacting configurations. The F87 calculations indicate that the N II 758.37 Å line as well as several other EUV spin changing lines in C I, N II, and O III have transition probabilities that are as large as allowed transitions. Lifetimes determined from the F87 oscillator strengths are compared to beam-foil lifetime measurements in Table 1. Note that the configurations are numbered consecutively in order of increasing energy (this notation is used throughout the paper). Some examples of the strength of the F87 spin-changing transitions are listed in Table 2.

The spin-changing 748.37 Å line ($2s^22p^2\ ^1D$–$2s^22p(^2P)3s\ ^3P^o$) in N II was first observed with the beam foil technique by Livingston et al. (1975). By observing this line they measured the life-time of the $2s^22p(^2P)3s\ ^3P^o$ configuration to be 0.60 ns. Other beam-foil lifetime measurements of this N II state agree reasonably with Livingston, Baudinet-Robinet, & Dumont (1975), and published values range from 0.58 ± 0.06 ns to 1.08 ± 0.09 ns (see Table 1), with most of the differences between these values now attributed to observation of different fine-structure populations rather than uncertainty in measurement. The beam foil experiments were not used to determine transition probabilities from configurations that have multiple depopulation routes, however, so the unusual strength of this transition was not noticed. Morrison, Cunningham, & Christensen (1983) have also observed this emission and have set a lower limit on the 748 Å/860 Å line intensity ratio.

Experimental measurements of electron excited N_2 described below verify the F87 results. As shown in Figure 1, the N II 748.38 Å line originates from the same upper configuration as the allowed N II 671 Å multiplet; we have determined the 748.37 Å branching ratio in an optically thin crossed beam observation. Since the F87 transition probabilities also give theoretical lifetimes in good agreement with beam-foil lifetime measurements (see Table 1), we conclude that the transition probability of the N II 748.37 Å line is $\sim 5 \times 10^8\ s^{-1}$.

In order to study how this type of intercombination line affects diagnostic data and collisional radiative quantities, we

TABLE 1

LIFETIMES OF SELECTED N II CONFIGURATIONS

Term Number	Configuration	Mean energy (cm^{-1})	Theoretical Lifetime (ns)	Observed Lifetimes (ns)
1.....	$2s^22p^2\ ^3P$	59.83	...	...
2.....	$2s^22p^2\ ^1D$	15316.20	2.5×10^{11}[a]	...
3.....	$2s^22p^2\ ^1S$	32688.80	8.7×10^{11}[a]	...
4.....	$2s2p^3\ ^5S^o$	46784.56	6.4×10^{6}[b] 3.3×10^{6}[d]	4.2×10^{6}[c]
5.....	$2s2p^3\ ^3D^o$	92246.43	2.2[e]	2.7[f], 2.8[g], 2.8[h], 3.2[i], 2.9[j], 2.9[k]
6.....	$2s2p^3\ ^3P^o$	109219.23	0.58[e]	0.82[f], 0.81[g], 0.77[i], 0.82[j], 0.96[k]
8.....	$2s^22p3s\ ^3P^o$	148975.09	0.69[e]	0.60[l], 0.90[m], 0.58[n], 0.90[o], 0.69[f], 1.01[k], 0.76[p], 0.82[i], 1.08[j]
9.....	$2s^22p3s\ ^1P^o$	149187.80	0.25[e]	0.22[q]
10.....	$2s2p^3\ ^3S^o$	155126.73	0.089[e]	0.10[i], 0.11[k]
19.....	$2s^22p3d\ ^1D^o$	187091.37	0.28[e]	0.37[i]

NOTE.—All observed lifetimes measured with the beam foil technique except *c*, which was measured with a radio frequency ion trap.

[a] Nussbaumer & Rusca 1979.
[b] Hibbert & Bates 1981.
[c] Knight 1982.
[d] Cowan, Hobbs, & York 1982.
[e] Fawcett 1987.
[f] Chang 1977.
[g] Dumont, Biemont, & Grevesse 1974.
[h] Berry et al. 1971.
[i] Buchet, Poulizac, & Carre 1972.
[j] Smith et al. 1970.
[k] Heroux 1967.
[l] Livingston et al. 1975; τ determined from 748 Å.
[m] Livingston et al. 1975; τ determined from 672 Å.
[n] Dumont et al. 1976; τ determined from 748 Å.
[o] Dumont et al. 1976; τ determined from 672 Å.
[p] Kernahan et al. 1974.
[q] Livingston et al. 1975.

have constructed our model of the electronic structure of N II using the F87 oscillator strengths whenever possible and earlier calculations for collision strengths and for transitions that F87 did not examine. The model employs a modified Born approximation to establish collision strengths in those cases in which more detailed calculations are not available. This model has been used in a collisional equilibrium calculation to obtain radiative cooling and rate coefficients and to examine how the temperature-diagnostic N II transitions at 6548 Å, 6583 Å, and 5755 Å could be affected by cascading through intercombination transitions such as 748.37 Å.

This N II model and recent measurements of N II emission excited through electron collisions with N_2, reported here and by Ajello et al. (1989) and James et al. (1990), place limits on excitation processes inferred from observations of atmospheric emission on the Earth and Titan. These issues are discussed briefly below.

TABLE 2

STRONG N II SPIN-CHANGING TRANSITIONS

Wavelength (Å)	Transition[a] ($j, i: J_j, J_j$)	Transition Probability[b] (s^{-1})
748.37.....	(8, 2: 1, 2)	4.80×10^{8}
860.20.....	(8, 3: 1, 0)	1.50×10^{7}
670.88.....	(9, 1: 1, 2)	5.43×10^{7}
670.51.....	(9, 1:1, 1)	3.96×10^{7}
670.30.....	(9, 1:1, 0)	4.95×10^{7}
534.87.....	(19, 1:2, 2)	1.87×10^{8}
534.64.....	(19, 1:2, 1)	9.10×10^{8}

[a] j = term number of upper configuration (from Table 1); i = term number of lower configuration; J = total angular momentum.
[b] Transition probabilities from Fawcett 1987.

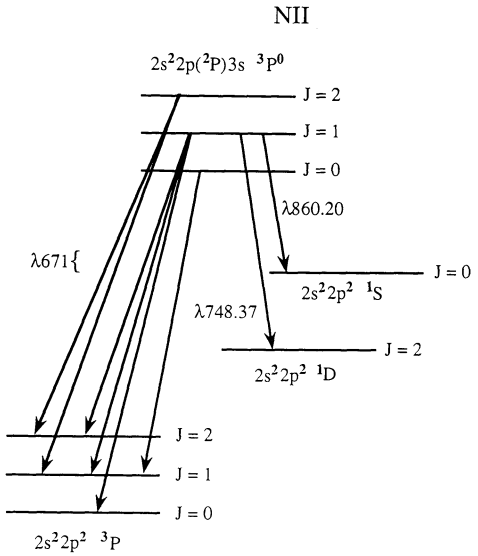

FIG. 1.—Partial Grotrian diagram of N II showing the remarkably strong spin-changing transition at 748.37 Å.

2. EXPERIMENTAL RESULTS

The apparatus has beeen described in detail by Ajello et al. (1989). The spectrometer is a medium resolution VUV Acton VM-521 with a dispersion of 8.3 Å mm^{-1} and a resolution of 0.3 Å (FWHM) with 20 μm entrance and exit slit widths. The observed point emission source is created in a crossed beam impact collision chamber in which a magnetically collimated electron beam (2–500 eV) impacts a gas beam formed by a capillary array at a background pressure that can be varied from 5×10^{-8} to 3×10^{-4} torr. The background pressure is chosen to provide optically thin conditions.

The calibration methods have been described in detail by Ajello et al. (1988). The relative intensity calibration curve for the spectrometer was obtained by observing the $n\,^1P^o n = 2,3,4$ Rydberg series of He as well as Ar I and Ar II multiplets. The entire spectrum was normalized by the absolute cross section of N I (1199.9 Å) produced by dissociative excitation as determined by the relative flow technique (Trajmar & Register 1984).

Ajello et al. (1989) have unambiguously identified N I, N II, and N III multiplets below 800 Å in the electron impact spectrum of N_2; consequently, we were able to observe the N II 671 Å and N II 748.37 Å lines in a medium resolution scan of the 660–760 Å region of the electron impact induced N_2 spectrum. The spectrum for 200 eV electron excitation of N_2 at 5.5×10^{-5} torr is shown in Figure 2. The statistical uncertainties in the features of interest are $\lesssim$4%. However, a much larger uncertainty (15%) is introduced by the calibration of the data.

3. DATA ANALYSIS

As can be seen from Figure 1, experimental determination of the 748.37 Å branching ratio is complicated by the fact that the 671 Å lines that originate from the $3s\,^3P^o(J = 1)$ level are blended with other fine-structure transitions from the $3s\,^3P^o(J = 0)$ and $3s\,^3P^o(J = 2)$ levels. These lines are resolvable with sufficiently high resolution. Although the resolution of our instrument is not high enough to separate each line in the feature, it is sufficient for reduction with a simple model, although the accuracy of the result is ultimately limited by resolution.

Because we produced the N II spectrum by simultaneous dissociation-ionization-excitation of N_2, we are unable to predict easily how the upper fine-structure levels in the dissociation fragments are populated, although we do obtain experimental rates. The branching ratio from a fine-structure level, however, is independent of population under optically thin conditions. Thus for term 8 (see Table 1), we can determine the observed branching ratio of ^1D–$^3P^o$ (748.37 Å) out of the $J = 1$ level and compare it to the branching ratio predicted by the F87 calculation.

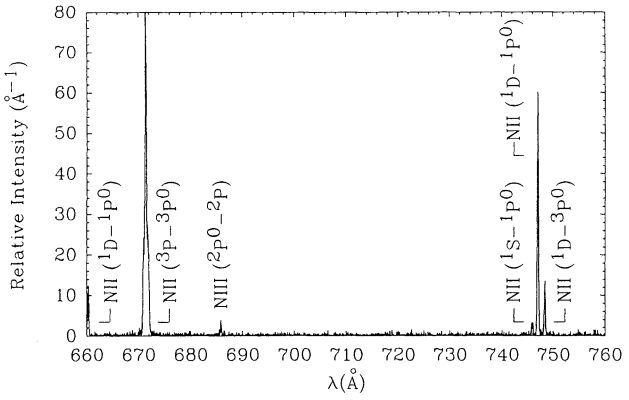

FIG. 2.—The optically thin emission spectrum of N_2 excited by electrons at 200 eV. N II and N III lines are detected with a resolution of 0.3 Å (FWHM).

In effect, we obtain the branching ratio directly from the observation by comparing the observed intensity ratio to the theoretical ratio:

$$\frac{I(748.37\ \text{Å})}{I(671\ \text{Å})} = \frac{A(8,\,2{:}1,\,2)}{A(8,\,1{:}1,\,J_i)}\,. \tag{1}$$

Here I is the relative intensity and $A(j, i{:}J_j, J_i)$ is the transition probability from upper level j (term number from Table 1) with total angular momentum J_j down to lower level i with total angular momentum J_i. We use this $(j,\ i{:}J_j,\ J_i)$ notation throughout the paper to identify fine-structure transitions. For convenience, we define $\vartheta_{ji} \equiv (j,\ i{:}J_j,\ J_i)$. In (1), $J_i = 0$, 1, or 2 (see Fig. 1), and the wavelengths of $(8,\ 1{:}1,\ J_i)$ transitions are 671.41, 671.63, and 672.00 Å, respectively. Since we cannot resolve the lines arising from the $J = 1$ level from the other lines, we use the following method to compare the F87 branching ratio to the observation. The fine-structure population rates of term 8 are obtained by scaling the theoretical branching ratios, $\mathscr{L}(\vartheta_{ji})$ (from F87), in the multiplets so that

$$I_o(8,\,1{:}J_j,\,J_i) = g(8{:}J_j)\mathscr{L}(8,\,1{:}J_j,\,J_i)\,, \tag{2}$$

where I_o is the volumetric emission rate, $g(j{:}J_j)$ is the population rate of level $(j{:}J_j)$, and

$$\mathscr{L}(\vartheta_{ji}) = \frac{A(\vartheta_{ji})}{A(j{:}J_j)}\,, \tag{3}$$

where $A(j{:}J_j) = \Sigma_{i:J_i} A(\vartheta_{ji})$. After we have determined $g(8{:}1)$ from the 671 Å multiplet, we solve for $I(8,\,2{:}1,\,2)$:

$$I(8,\,2{:}1,\,2) = g(8{:}1)\mathscr{L}(8,\,2{:}1,\,2)\,. \tag{4}$$

Finally, we compare this $I(8,\,2{:}1,\,2)$ predicted by F87 to the observed intensity. If the $I(8,\,2{:}1,\,2)$ predicted by equation (4) compares well to the observed emission, then the branching ratio is correct to within the uncertainty of the fit.

In order to compare the observed spectrum to the theory, the branching ratios were convolved with a trapezoidal transmission function (FWHM = 0.3 Å, peak full width = 0.09 Å) appropriate for the instrument. The relative line strengths of the 671 Å multiplet lines (represented by the convoluted branching ratios) are plotted against the spectrometric data in Figure 3. All lines originating from upper terms with the same J-value are scaled together as noted above. Although the $g(j{:}J_j)$ values are free parameters, our data allow very little latitude. Only the $J = 2$ component can account for the emission observed in the 670.8–671.1 Å region and must be scaled appropriately in order to obtain a good fit to that part of the feature. Similarly, only the $J = 1$ component can account for emission in the 672.1–672.3 Å region; consequently, the scaling factor of this component is also tightly constrained. Finally, the $J = 0$ component must be scaled to fit whatever remains in the observed spectrum after the two constraining regions have been fitted.

The theoretically predicted 671 Å feature obtained from the branching ratios in Table 3 is plotted against the data in Figure 4*a*, and $I(8,\,2{:}1,\,2)$ obtained from equation (4) is plotted against the data in Figure 4*b*. The model appears to fit the data well. In

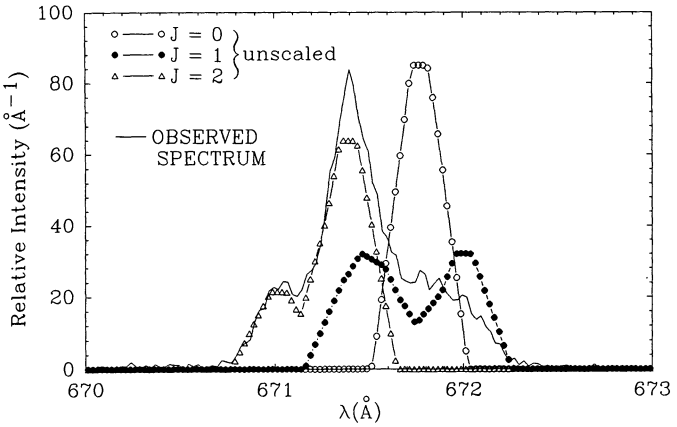

FIG. 3.—Model spectra of the N II 671 Å multiplet fine structure showing the separated transitions from the upper state levels, convolved with the transmission function but not scaled by the population rates, compared to the experimental data. The transmission function is a trapezoid with FWHM = 0.3 Å and peak width = 0.09 Å.

order to compare the model to the data quantitatively, we define

$$B_1 = \frac{\int_{\lambda_3}^{\lambda_4} I_o(\lambda)d\lambda}{\int_{\lambda_1}^{\lambda_2} I_o(\lambda)d\lambda}, \quad (5)$$

where $\lambda_1 = 670.76$ Å, $\lambda_2 = 672.26$ Å, $\lambda_3 = 748.11$ Å, and $\lambda_4 = 748.61$ Å. According to the data, $B_1 = 0.0826$, while, according to the model, $B_1 = 0.0802$.

We also estimate the $I_0(8, 2{:}1, 2)/I_0(8, 1{:}1, 2)$ fine-structure intensity ratio by integrating over the 748.37 Å line and *part* of the 672.00 Å feature. Emission in the 672.1–672.3 Å region can be due to the (8, 1:1, 2) transition. Unfortunately, this line is partially blended with the (8, 1:0, 1), (8, 1:1, 1), and (8, 1:1, 0) transitions so we cannot integrate over the entire (8, 1:1, 2) line (see Fig. 3). Instead, we integrate over the unblended part of the (8, 1:1, 2) line between 672.05 and 672.25 Å and then use our estimation of the instrument's transmission function to reconstruct the rest of the emission. Since this region comprises 32.2% of the entire (8, 1:1, 2) line, we estimate that the integral over the entire (8, 1:1, 2) line is

$$I_0(8, 1{:}1, 2) = \frac{1}{0.322}\int_{672.05}^{672.25} I_0(\lambda)d\lambda . \quad (6)$$

After reconstructing the (8, 1:1, 2) line in this way, we find that $I_0(8, 2{:}1, 2)/I_0(8, 1{:}1, 2) = 0.64$. According to the F87 calculation $A(8, 2{:}1, 2)/A(8, 1{:}1, 2) = 0.96$.

In a low-resolution experiment (FWHM = 5 Å), Ajello et al. (1989) have determined the emission cross sections of the 671 and 747 Å features produced by 200 eV electron impact upon N_2. We have used the intensities of the components in the 671 Å multiplet (determined from eq. [2]) and the unblended 746, 747, and 748 Å line intensities to partition the Ajello et al. (1989) cross sections among the 671 and 747 Å fine-structure transitions. These emission cross sections are given in Table 3. The excitation cross sections are related to the emission cross sections by

$$\sigma_{ex}(j{:}J_j) = \sum_{i:J_i} \sigma_{ex}(\vartheta_{ij}) = \frac{\sigma_{em}(j{:}J_j)}{\mathscr{L}(\vartheta_{ji})}, \quad (7)$$

and the population rate in $cm^{-3}\ s^{-1}$ is given by

$$g(j{:}J_j) = \mathscr{F}_e\, \sigma_{ex}(j{:}J_j)N(i), \quad (8)$$

where $\mathscr{F}_e$ is the electron flux and $N(i)$ is the population of the ground state.

4. COLLISIONAL EQUILIBRIUM CALCULATIONS

We have constructed an electronic structure model for N II which we have employed in collisional equilibrium calculations of radiative cooling coefficients (ρ), rate coefficients (k), and temperature diagnostic line ratios.

The details of the iterative method have been described by Shemansky & Smith (1981). Our computational method differs from the one described by Osterbrock (1989) in the following ways: (1) we employ collision strengths which are functions of temperature (or electron energy) instead of using a constant mean collision strength and (2) our calculation includes the first 73 fine-structure levels (up to $E = 211389.75\ cm^{-1}$) instead of just the first five. The calculation is based on the assumption that the species is in a steady state collisional equi-

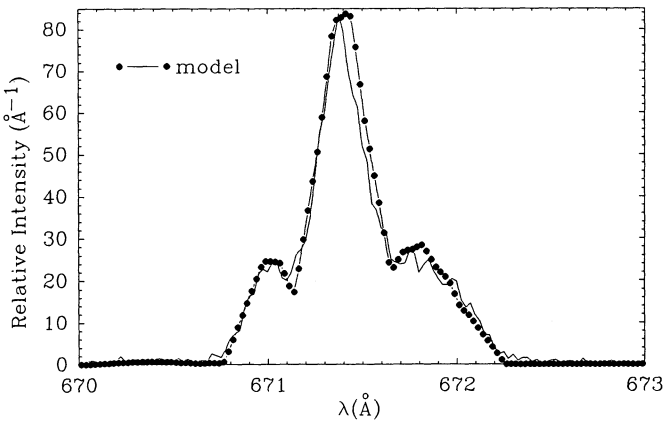

FIG. 4a

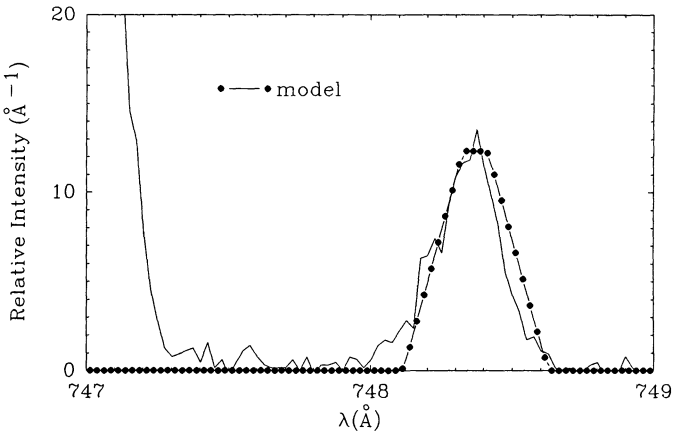

FIG. 4b

FIG. 4.—(*a*) Model of the N II 671 Å feature plotted against the observed spectrum. The model is produced by scaling the model components shown in Fig. 3 by the population rates, $g(j{:}J_j)$. (*b*) N II 748.37 Å line predicted by eq. (4) plotted against the observed spectrum. The population rate, $g(8{:}1)$, is obtained from the models shown in (*a*).

TABLE 3

BRANCHING RATIOS AND CROSS SECTIONS OF TRANSITIONS FROM N II TERMS 8 AND 9

Transition (j, i:J_j, J_i)	$\lambda(j, i{:}J_j, J_i)$ (Å)	$\mathscr{L}$	$\sigma_{ex}(i, j{:}J_i, J_j)$[a] ($10^{-19}$ cm^2)	$\sigma_{em}(j, i{:}J_j, J_i)$[a] ($10^{-19}$ cm^2)	$\sigma_{ex}(i, j{:}J_i, J_j)$[b] ($10^{-19}$ cm^2)	$\sigma_{em}(j, i{:}J_j, J_i)$[b] ($10^{-19}$ cm^2)
(8, 1:0, 1).....	671.77	1.000	0.91	0.91	6.06	6.06
(8, 1:1, 2).....	672.00	0.299	1.79	0.54	13.7	4.11
(8, 1:1, 1).....	671.63	0.173	1.79	0.31	13.7	2.38
(8, 1:1, 0).....	671.41	0.234	1.79	0.42	13.7	3.22
(8, 1:2, 2).....	671.39	0.749	4.00	3.01	15.9	11.9
(8, 1:2, 1).....	671.02	0.251	4.00	1.01	15.9	4.00
(8, 2:1, 2).....	748.37	0.285	1.79	0.48	13.7	3.93
(8, 3:1, 0).....	860.20	0.009	1.79	0.015	13.7	0.12
(9, 1:1, 2).....	670.88	0.014	2.60	0.04	1.44	0.019
(9, 1:1, 1).....	670.51	0.010	2.60	0.03	1.44	0.014
(9, 1:1, 0).....	670.30	0.012	2.60	0.03	1.44	0.018
(9, 2:1, 2).....	746.98	0.933	2.60	2.27	1.44	1.34
(9, 3:1, 0).....	858.38	0.032	2.60	0.08	1.44	0.045

[a] $e^- + N_2(R1)$, $E_e = 200$ eV.
[b] $e^- + N^+(R2)$, $E_e = 200$ eV, $[e^-] = 1000$ cm^{-3}.

librium so that for each of the levels $j = 1, 39$ the equilibrium equations are

$$\sum_{i<j} N(i{:}J_j)P(\vartheta_{ij}) + \sum_{k>j} N(k{:}J_k)L(\vartheta_{kj}) + \sum_{k>j} N(k{:}J_k)A(\vartheta_{kj}) = \sum_{i<j} N(j{:}J_j)L(\vartheta_{ji}) + \sum_{i<j} N(j{:}J_j)A(\vartheta_{ji}) + \sum_{k>j} N(j{:}J_j)P(\vartheta_{jk}) , \quad (9)$$

where A is the radiative transition probability, $L(\vartheta_{ji})$ is the loss rate from level j down to level i due to collisional de-excitation, and $P(\vartheta_{ij})$ is the production rate from level i up to level j due to collisional excitation. Thus the left side of equation (9) describes how level j is populated through collisional excitation from lower levels and nonradiative and radiative cascades from higher levels, and the right side of equation (9) describes the depopulation of level j through collisional deexcitation, spontaneous radiative decay, and collisional excitation up to higher levels. $N(j{:}J_j)$ is the number density of ions in the fine-structure level $(j{:}J_j)$ normalized so that

$$\sum_{j:J_j} N(j{:}J_j) = 1 .$$

That is, $N(j{:}J_j)$ is the relative population of ions in a particular fine-structure level. The production rate of a level $(j{:}J_j)$ per source ion initially in the level $(i{:}J_i)$ and the related collisional loss rate can be described by the following equations (see Osterbrock 1989):

$$P(\vartheta_{ij}) = [e^-] \frac{8.629 \times 10^{-6}}{T_e^{1/2}} \left[\frac{\bar{\Omega}(\vartheta_{ij})}{\omega_{J_i}}\right] \exp\left(-\frac{E_{ij}}{kT_e}\right) \text{s}^{-1} , \quad (10)$$

$$L(\vartheta_{ji}) = [e^-] \frac{8.629 \times 10^{-6}}{T_e^{1/2}} \left[\frac{\bar{\Omega}(\vartheta_{ji})}{\omega_{J_j}}\right] \text{s}^{-1} , \quad (11)$$

where T_e is the electron temperature and $[e^-]$ is the electron number density, $\bar{\Omega}(\vartheta_{ij})$ is the thermally averaged fine-structure collision strength (a function of T_e), ω_{J_i} and ω_{J_j} are the lower and upper level fine-structure degeneracies, and E_{ij} is the energy of the transition. Equation (9) is a matrix equation which is solved iteratively, as described by Shemansky & Smith (1981), for all $N(j{:}J_j)$. After the relative populations of the fine-structure levels have been determined in this way, the fine-structure radiative cooling and rate coefficients are calculated by

$$\rho(\vartheta_{ji}) = A(\vartheta_{ji})h\nu\left[\frac{N(j{:}J_j)}{[\text{N II}][e^-]}\right] , \quad (12)$$

$$k(\vartheta_{ji}) = A(\vartheta_{ji})\left[\frac{N(j{:}J_j)}{[\text{N II}][e^-]}\right] . \quad (13)$$

Since

$$\sum_{j:J_j} N(j{:}J_j) = 1, [\text{N II}] = 1 .$$

The total coefficients for transitions between two configurations are obtained by summing equation (12) or (13) over all fine-structure transitions between the terms, and the total radiative cooling coefficient for the species is obtained by summing the coefficients for all transitions between all of the configurations in the model.

Calculations have been made over the temperature range $4000 \leq T_e \leq 1 \times 10^6$ K for two electron densities, $[e^-] = 100$ cm^{-3} and $[e^-] = 1 \times 10^{10}$ cm^{-3}. The electronic structure model contains the first 39 terms of N II (i.e., the first 73 fine-structure levels) up to $E = 211389.75$ cm^{-1} and contains 381 excitation/de-excitation channels. Fine-structure level energies were obtained from Bashkin & Stoner (1975), except for the energies of the ^5S configuration (term 4) which were obtained from Eriksson (1983). Transition probabilities were obtained from F87 whenever possible. The references in Table 1 as well as Wiese, Smith, & Glennon (1966) and Wiese & Martin (1980) were used for other transitions. When transition probabilities were not available in the literature, they were calculated with the Bates & Damgaard (1949) Coulomb approximation. An analytical function, similar to that given by Shemansky et al. (1985) but adapted for ions, was fitted to the collision strength data for each transition. Collision strength data for the first 13 levels were obtained from Seaton (1975) and Jackson (1973), and a modified Born approximation was used to calculate the remaining collision strengths. Our results are shown in Figures 5–8.

5. DISCUSSION

5.1. *Results*

A comparison of the spectrum predicted by the F87 oscillator strengths to our observation (see Fig. 4) indicates that at

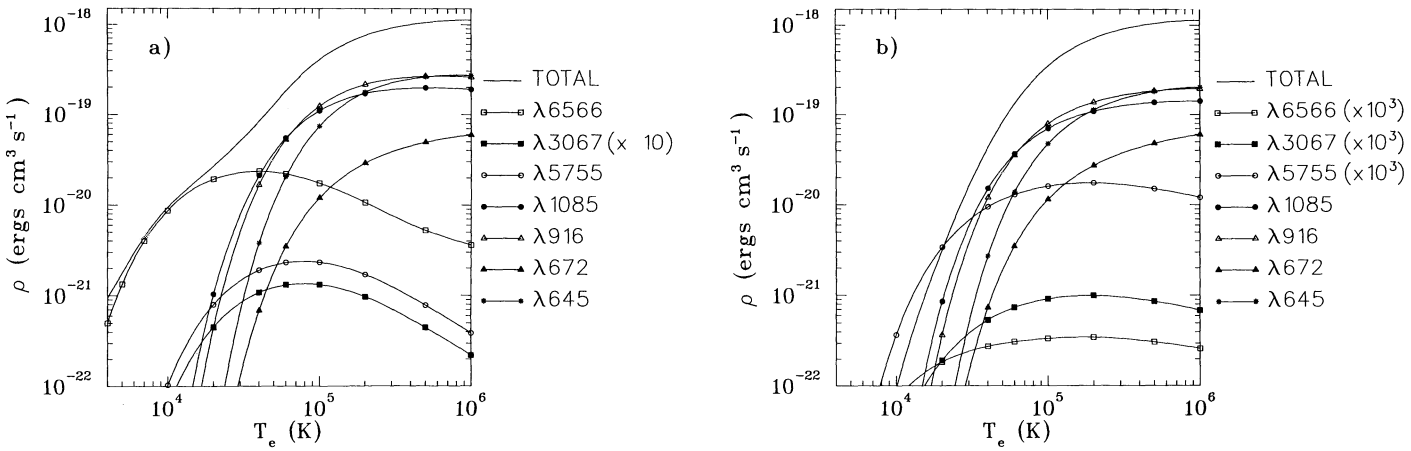

FIG. 5.—Radiative cooling coefficients for N II in collisional equilibrium with (*a*) $[e^-] = 100\ \mathrm{cm}^{-3}$, and (*b*) $[e^-] = 10^{10}\ \mathrm{cm}^{-3}$. Optical transitions are indicated by their average air wavelengths, and ultraviolet transitions are indicated by average vacuum wavelengths.

least one spin changing transition in N II, the 748.37 Å line, is indeed as strong as an allowed electric dipole transition. A comparison of the values of B_1 (eq. [5]) given by the data and the model shows that the theoretical and experimental line ratios agree to within 4%. However, since the uncertainty of the data calibration is much larger, the closeness of the fit is fortuitous. The good agreement between the $I(8, 2{:}1, 2)$ predicted by equation (4) and the observed $I_0(8, 2{:}1, 2)$ implies that $\mathscr{L}(8, 2{:}1, 2) = 0.29 \pm 0.15$. Our second method of comparing the F87 calculations to the data produces theoretical and experimental line intensity ratios that disagree by ~33%. However, the second method is somewhat unreliable because (1) integration was conducted over only a portion of the $I_0(8, 1{:}1, 2)$ line so the statistical uncertainty rises, and (2), although a trapezoidal point-spread function is a suitable line shape for modeling purposes, it can be seen from Figure 4 that the true instrument function may not be a perfect trapezoid; consequently, our reconstructed (8, 1:1, 2) line may be too strong. Beam-foil lifetime measurements based on observations of the 671 Å multiplet may be problematic because of the blending of lines from different fine-structure levels. F87 indicates that the lifetime of the $J = 1$ level is ~30% shorter than the lifetimes of the $J = 0$ and 2 levels of term 8. Lifetime measurements based on 748 Å are free of this problem because they detect emissions from the $J = 1$ level only. The F87 lifetime for term 8, $J = 1$, is in excellent agreement with the beam-foil lifetime measurements based on 748 Å: F87 gives $\tau(8, 1) = 0.59$ ns compared to $\tau(8, 1) = 0.60$ ns from Livingston et al. (1975) and 0.58 ns from Dumont, Baudinet-Robinet, & Livingston (1976).

This particular transition may be unique. Goldbach, Martin, & Nollez (1989) have measured oscillator strengths of two C I spin-forbidden transitions, and their measurements are not in good agreement with the F87 calculation. Goldbach, Martin, & Nollez (1989) report gf values of 0.0028 ± 21% for C I 1467.88 Å and $gf = 0.0034 \pm 20\%$ for C I 1470.09 Å. The oscillator strengths given in F87 for these transitions are, respectively, $gf = 0.007$ and $gf = 0.060$. We note, however, that oscillator strengths of neutral species are generally more difficult to calculate accurately. Further studies of these intercombination transitions would be useful.

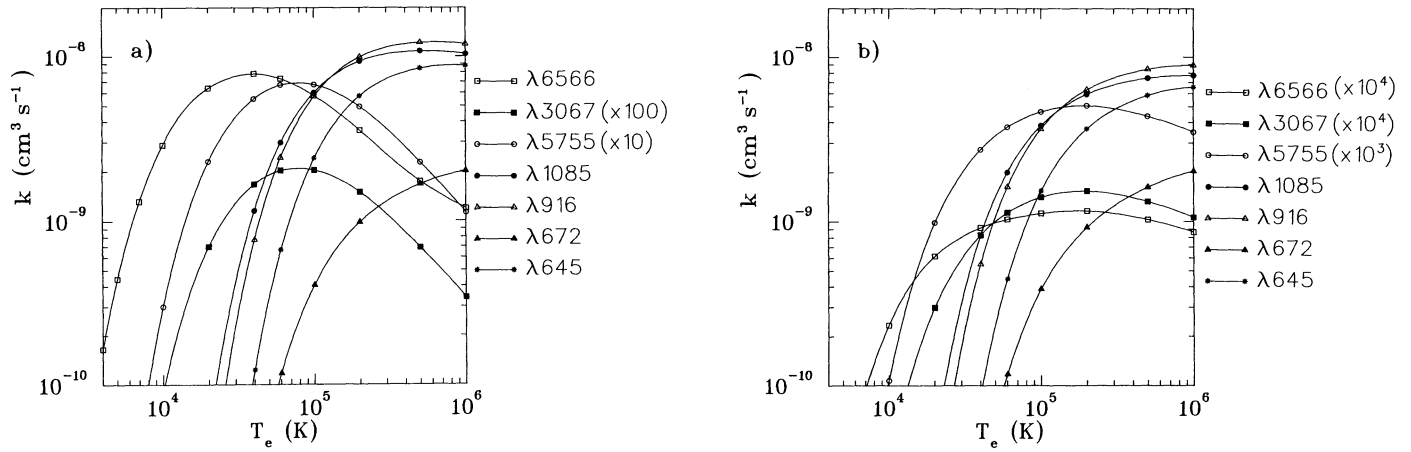

FIG. 6.—Rate coefficients for N II in collisional equilibrium with (*a*) $[e^-] = 100\ \mathrm{cm}^{-3}$, and (*b*) $[e^-] = 10^{10}\ \mathrm{cm}^{-3}$. See Fig. 5.

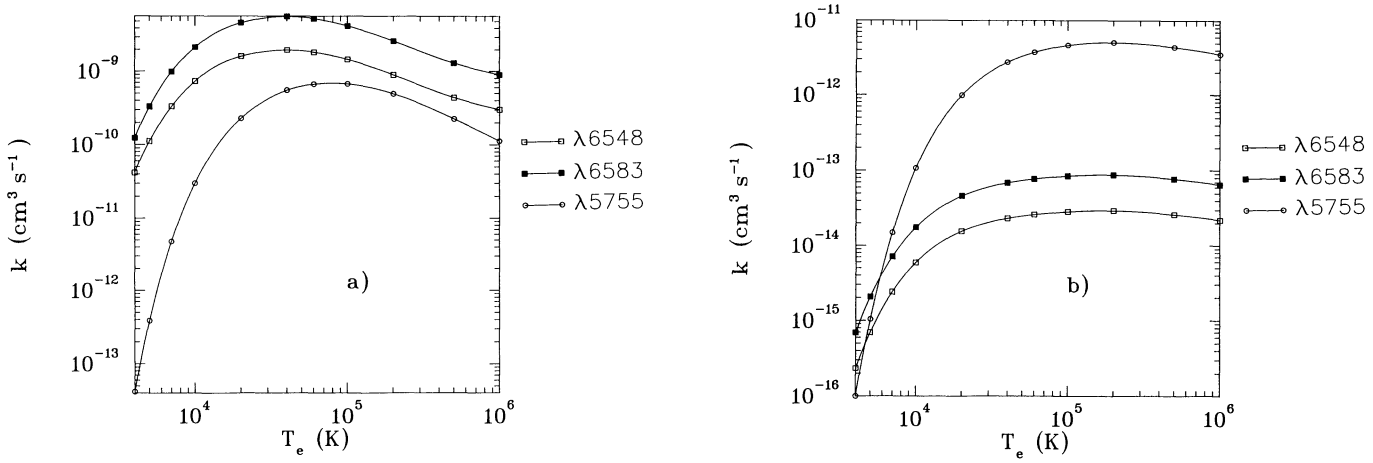

FIG. 7.—Fine-structure rate coefficients for the N II temperature diagnostic lines (^3P–^1D and ^1D–^1S) with (*a*) $[e^-] = 100$ cm^{-3}, and (*b*) $[e^-] = 10^{10}$ cm^{-3}

5.2. *Astrophysical Applications*

We were originally motivated to build our N II electronic structure model in order to reexamine the *Voyager* Ultraviolet Spectrometer (UVS) observations of Titan. Since the UVS operates from 500–1700 Å and the emissions are believed to be electron excited (Strobel & Shemansky 1982), a moderately extensive model is needed in order to study the EUV emissions accurately. Seventy-three fine-structure levels are probably more than necessary for typical astrophysical plasmas (e.g., planetary nebulae, H II regions) which are usually too cool to excite many higher energy terms; nevertheless, there are some problems that may require a larger number of terms, particularly to determine radiative cooling efficiencies (e.g., supernova remnants, AGN emission-line regions).

Emission spectra have been used for a number of years to study the physical conditions in astrophysical (i.e., hot and thin) plasmas. The various techniques of emission-line study are well-known and have been discussed (see Osterbrock 1989; Raymond 1988); they range in complexity from simple photoionization equilibrium calculations and thermal equilibrium calculations to models that include dynamical considerations such as shock and ionization fronts. Processes that are usually included in these calculations are photoionization, photoexcitation, collisional ionization and excitation, radiative and dielectronic recombination, and thermal bremsstrahlung. For X-ray emission, UV emission, and radiative cooling, collisional processes are often dominant.

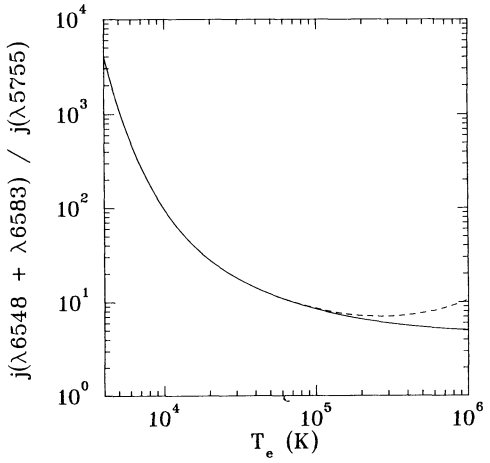

FIG. 8.—The N II temperature diagnostic ratio for the low-density case ($[e^-] = 100$ cm^{-3}). Dashed curve was calculated with a 73 level model that includes the strong intercombination transitions, while the solid curve was calculated with the same model after the intercombination transitions were removed. Solid curve is nearly identical to the results obtained in a five-level calculation.

Radiative cooling rates have previously been calculated for nitrogen by Tarter (1977), Raymond, Cox, & Smith (1976), Dalgarno & McCray (1972), Cox & Daltabuit (1971), Cox & Tucker (1969), and Jordan (1969). Nitrogen is also included in the photoionization equilibrium code CLOUDY (Ferland & Rees 1988). In general, these papers fold radiative cooling coefficients for several stages of ionization of a particular species into a single cooling curve by assuming ionization equilibrium. They assume, for example, that the ratio of successive ionization stages is the sum of the collisional and autoionization rates over the sum of the radiative and dielectronic recombination rates (see Tarter 1977). While this is an entirely reasonable procedure, it can be advantageous to separate each ion into individual cooling coefficient curves so that when improved calculations of ionization or recombination rates become available, the cooling data can be easily updated. Radiative cooling coefficients given by equation (12) and rate coefficients (13) are shown in Figures 5 and 6 for two electron densities, $[e^-] = 100$ cm^{-3} and $[e^-] = 1 \times 10^{10}$ cm^{-3}. The effect of electron density on radiative efficiency is strong below $T_e = 5 \times 10^4$ K (see Figs. 5 and 6). It is not always clear how many levels are included in previous cooling calculations. The accuracy of radiative cooling coefficients is compromised in calculations that include *only* the strongest UV lines. At high temperatures the major EUV transitions in the current calculation at 1085, 916, and 645 Å account for only ~65% of the total radiated energy. A potential problem with the accuracy of the current calculations occurs when $T_e < 10^5$ K. Electron exchange collision strengths for a number of states are not available, and possible dipole components of heavily mixed singlet states are not included. The radiative cooling curves given here may therefore be significantly underestimated at lower temperatures in spite of the inclusion of more states.

For most species subject to *LS*-coupling, line diagnostics can be computed satisfactorily with five-level calculations as described by Osterbrock (1989). However, such calculations may be insufficient for C I, N II, and O III due to the spin-forbidden transitions reported by F87. For sufficiently hot plasmas, these intercombination lines could boost the populations of the lowest singlet states through cascading from the triplet system which, in turn, could affect the temperature diagnostic N II emissions at 6548, 6583, and 5755 Å. We have used our model to address this question, and the results are shown in Figures 7 and 8. As expected, Figure 7*b* shows that these lines are probably not detectable in the high-density case because of collisional de-excitation. Nevertheless, it is interesting to compare the structure of the rate coefficients in the low-density case to that in the high-density case. In Figure 7*a*, the 6548 and 6583 Å curves [the (2, 1:2, 1) and (2, 1:2, 2) transitions] become slightly concave at higher energies. This is due to boosting of the term 2 population through intercombination cascading. F87 does report two EUV intercombination transitions that feed term 3, but (8, 3:1, 0) competes with 671 and 748 Å while the other transition comes from a high-energy term; consequently, the 5755 Å curve [the (3, 2:0, 2) transition] is not significantly influenced by intercombination cascading. In Figure 7*b*, we see that these spin-forbidden transitions have no effect on any of the transitions when de-excitation is dominant. From Figure 8 we see that cascading does not affect the line ratio for $T_e < 10^5$ K, and the line ratio is changed by a factor of 2 at $T_e \sim 10^6$ K. If diffusion loss rates are negligible, nitrogen equilibrates at N VI and N VII at 10^6 K (Shapiro & Moore 1976; Cox & Tucker 1969). However, N II in active galactic nuclei could be excited by high-energy electrons and photons. In this environment, K shell photoionization and the corresponding Auger processes produce high-energy free electrons. Since the Coulomb-scattering cross section goes as E^{-2}, these high-energy electrons are not as rapidly thermalized by Coulomb collisions as are free electrons produced by normal photoionization and could impact N II (and other heavy elements) in active galactic nuclei transition regions, causing excitation or ionization instead of heating the gas. If this happens, then models may need to include the F87 intercombination cascading in order to calculate N II line intensities correctly. Supernova remnants provide another situation in which N II could be exposed to high-energy electrons. Blair & Raymond (1984) have found that when a shock wave enters an interstellar cloud, the pre-shock gas is at first severely underionized. This could allow N II to exist in a hot gas at the front of a shock.

We find that the diagnostic line ratio shown in Figure 8 remains basically the same at electron temperatures below 10^5 K, independent of the presence of intercombination lines and levels higher than term 5. A five-level calculation is therefore almost always sufficient for these optical line ratio diagnostics.

5.3. *Earth Airglow*

One of the outstanding issues in the airglow, very bright N II 1085 Å emission, was first recognized in early EUV observations by Christensen (1976). Model calculations for photoelectron excitation of N_2 to produce N II 1085 Å emission,

$$N_2 + e^- \rightarrow N^+(*) + N + 2e^-, \qquad \text{(R1)}$$

were a factor of ~8 weaker than the measurements (Christensen 1976). Observations since the Christensen (1976) experiment have produced results consistent with his conclusion (see Eastes et al. 1985; Chakrabarti et al. 1983; Gentieu et al. 1981; Gentieu et al. 1979). Some of the airglow and aurora observations are summarized in Table 4. The recent cross section measurements for dissociative ionization-excitation of N_2 (James et al. 1990) establish a smaller cross section for N II 1085 Å emission, aggravating a possible solution through this excitation process. Direct electron excitation of N II or resonance scattering of solar radiation appears to be improbable because of the low abundance of N II in the ionosphere. The airglow N II 916 Å emission is also anomalously intense: the

TABLE 4

RELATIVE EMISSION RATES FOR EUV NITROGEN TRANSITIONS ON EARTH AND TITAN

Source	LBH/1085	916/1085	670/1085	670/747
Earth airglow[a]	21.91	1.87	0.42	...
Earth airglow[b]	...	~2.2	~0.8	~0.7
Earth airglow[c]	7.40	0.37	0.01	>1.6
Earth airglow[d]	19.76	1.32	0.50	...
Earth airglow[e]	...	1.63	...	...
Earth airglow[f]	...	0.39	...	...
Earth airglow[g]	15.74	...	...	...
Earth airglow[h]	10.37	...	...	...
Earth aurora[i]	...	0.23	...	...
Earth aurora[j]	4.43	0.13	...	...
Earth aurora[k]	...	0.13	...	...
Earth aurora[l]	...	0.09	...	...
Earth aurora[m]	15.15	...	...	...
Titan[n]	8	0.08	0.07	0.38
(R1)[o]	407	0.15	0.065	2.63
(R1)[p]	3	0.26	0.11	2.17
(R1)[q]	7.2	0.21	0.11	2.22
(R1)[r]	17	0.18	0.11	2.27
(R2)[o]	...	0.95	0.078	6.67
(R2)[p]	...	1.2	0.29	6.67
(R2)[r]	...	1.1	0.15	6.67

[a] Morrison et al. 1990. 1985 January 17, zenith angle = 70°–90°, altitude = 140–169 km (total LBH intensity determined from observed (5, 2) 1382 Å and (2, 0) 1384 Å emissions).

[b] Chakrabarti et al. 1983. 1979 March 20–22, zenith angle = 30°–80°, altitude = 600 km.

[c] Chakrabarti et al. 1983. 1979 March 5–15, zenith angle = 120°–150°, altitude = 600 km.

[d] Gentieu et al. 1979, 1981. 1978 January 9, zenith angle = 56°, altitude ≥ 210 km.

[e] Christensen 1976. 1975 September 24, zenith angle = 44°–50°, altitude = 210–240 km.

[f] Christensen 1976. 1975 September 24, zenith angle = 100°–110°, altitude = 276–263 km.

[g] Gentieu et al. 1981. 1980 June 27, zenith angle = 90°, altitude = 220 km.

[h] Eastes et al. 1985. 1980 June 27, zenith angle = 98°, altitude = 240–260 km.

[i] Gentieu et al. 1989. 1981 December 7, viewing ±60° to the nadir, altitude ≥380 km.

[j] Chakrabarti 1986. 1979 March 22, zenith angle = 120°–150°, altitude = 600 km (total LBH intensity determined from observed (4, 0) 1325 Å emission).

[k] Park et al. 1977. 1976 March 26, zenith-viewing, altitude = 130–170 km.

[l] Park et al. 1977. 1976 March 26, side-looking, altitude = 170–175 km.

[m] Meier et al. 1982. 1978 March 29, side-looking, altitude = 150 km (total LBH intensity determined from observed (4, 0) 1325 Å emission).

[n] Strobel & Shemansky 1982. *Voyager 1* disk average.

[o] Photoelectron excitation.

[p] $T_e = 10^6$ K.

[q] $T_e = 5 \times 10^5$ K.

[r] $T_e = 3 \times 10^5$ K.

N II 916 Å/1085 Å ratio is a factor of ~10 greater than the ratio expected from (R1) at 100 eV (see Table 4). The relative strength of the N II 1085 Å feature in aurorae and auroral N II 916 Å/1085 Å ratios, however, are generally consistent with (R1) (Gentieu et al. 1989; Chakrabarti 1986; Meier et al. 1982; Park, Feldman, & Fastie 1977; see Table 4). The laboratory work predicts that N II 670 Å should also be present with comparable strength for (R1) at 100 eV, but the airglow and auroral observations do not always show a feature at this wavelength. However, the weakness of this line may be expected because of extinction by the ionization continuum of foreground gas. The feature N II 747 Å in (R1) is about half the strength of N II 916 Å and N II 670 Å. A rather weak feature at 747 Å has been reported in atmospheric spectra but, along with 670 Å, has been attributed to O II and O I (Morrison et al. 1990; Gentieu et al. 1989, 1984; Gentieu, Feldman, & Meier 1979; Chakrabarti et al. 1983; Feldman et al. 1981). The short-wavelength oxygen features also appear to show anomalously large emission rates compared to expectation. Feldman et al. (1981) argue that the O II 834 Å feature is produced primarily by direct photoionization of O I. However, the O II 617 Å and 673 Å lines cannot be produced with comparable efficiency by the same process because of the requirement for simultaneous excitation of two electrons. Chakrabarti et al. (1983) have suggested, based upon the disagreement between their measured 617 Å/673 Å intensity ratio and the experimental and theoretical ratios (see Table 2 in Chakrabarti et al. 1983), that some of the 670 Å feature is attributable to N II. Assigning the 747 Å feature and a portion of 670 Å to N II is consistent with the strength of the 916 Å and 1085 Å lines. However, the Chakrabarti et al. (1983) measurements show a 617 Å/670 Å intensity ratio that is too large for the known branching in O II. Since extinction cannot affect this ratio, we are left with a dilemma, and the features below 750 Å cannot be explained with current rate processes for either oxygen or nitrogen species.

At 200 eV, the feature at 747 Å produced by (R1) is dominated by the N II ^1D–$^1P^o$ transition (see Fig. 2), whereas, according to our model calculations, the intercombination line ^1D–$^3P^o$ at 748 Å dominates in the reaction

$$N^+ + e^- \rightarrow N^+(*) + e^- . \quad (R2)$$

The N II ($^1P^o$) state is only weakly excited in (R2). The relationship between the 670 and 747 Å features in the nitrogen spectrum is therefore diagnostic of the relative contributions of (R1) and (R2) to the emission, essentially independent of the electron temperature. Table 3 shows a comparison of the cross sections for (R1) and (R2) at 200 eV, and Figure 9 shows a comparison of spectra produced by (R1) and (R2) at 200 eV. A rough estimate of rate coefficients for (R1) has been calculated and inserted into Table 4 on the basis of the Ajello et al. (1989) cross section and threshold measurements. The relative intensities of the N_2 Lyman-Birge-Hopfield (LBH) bands and the N II 1085 Å multiplet are sensitive to the electron temperature, in (R1). The LBH/1085 Å brightness ratio observed in the airglow ranges from ~10 to ~20. Our rough estimate of the rate coefficients for (R1) indicates that the expected ratio is ~400 for photoelectrons reacting with N_2. We conclude that on the whole, the airglow data could be consistent in spectral content (N II 670 Å, 474 Å, 916 Å, 1085 Å; N_2 LBH) with emission produced by (R1), but with electron temperatures typical of auroral conditions, although the 916 Å feature remains anomalously bright in most observations. The reaction

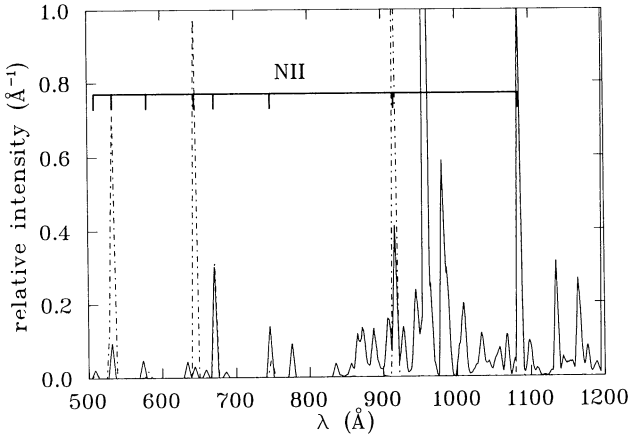

FIG. 9.—Laboratory spectrum of N_2 (*solid line*) compared to a model of N II (*dashed line*), both excited by 200 eV electrons. The spectral resolution is 5 Å (FWHM). The model was calculated with $[e^-] = 1000$ cm^{-3}, and the spectra are normalized at the N II 1085 Å line.

$$N + e^- \rightarrow N^+(*) + e^- \quad (R3)$$

can produce the N II 1085 Å line with a single electron excitation. However, production of the N II 670 Å and 747 Å features in (R3) is expected to be very inefficient because the process involves the simultaneous excitation of two electrons and because, again, the abundance of atomic nitrogen is low in the upper ionosphere.

The role of solar photons in exciting the N II emissions was considered briefly initially by Christensen (1976) with the conclusion that this source was unlikely to be a strong contributor. However, this possibility has not been considered quantitatively, and photoionization-dissociation-excitation of N_2 may be a plausible mechanism for production of the 1085 Å emission:

$$N_2 + h\nu \rightarrow N^+(*) + N + e^- . \quad (R4)$$

The altitude profiles of N II 1085 Å track the N_2 LBH profiles (R. R. Meier, private communication) which suggests that the N II excitation mechanism involves N_2 (as opposed to N I or N II). The LBH emissions are electric dipole forbidden, so if (R4) is the source, then the photoelectrons produced by (R4) must go on to excite the N_2 LBH bands. However, this proportionality is not unique to photons, and direct electron excitation will show the same effect. The dominant source of photoionization at energies above 37 eV is the He^+ line at 303.8 Å. If we use the measured cross section for N_2^+ B for (R4), in combination with yields for electron excitation (Appendix A), we obtain estimates of 0.015 and 0.003 for the yields of N II 1085 and 916 Å emission produced by 303.8 Å photons. Using a solar flux of $\pi F = 3 \times 10^{10}$ cm^{-2} s^{-1} we predict 170 R in N II 1085 Å for observations in the nadir from above the atmosphere, using an N_2 extinction partitioning factor of 0.37. Near solar maximum (1979) the observed quantity is typically 500 R (Chakrabarti et al. 1983). Observations by Christensen (1976) in 1975 observing at 44°–50° zenith angle (solar zenith angle 74°) from ~220 km gave a value of 35 R, while we predict ~10 R. However, the N II 916 Å emission is generally reported at values ~2 times brighter than the 1085 Å feature, whereas it is expected to be much weaker, based on the current estimate of yield.

The strength of the 916 Å airglow emission may be due in part to blending, but observers have attempted to separate the line from the underlying bands. The rocket measurements are generally low resolution; the N II 916 Å line may be blended with N_2 $b'(11, 1)$ transition at 915.3 Å as well as N I 910 Å. Observations in the zenith from above 200 km generally show the N II 916 Å line at double the strength of the N II 1085 Å feature. Nadir observations such as those of Chakrabarti et al. (1983) show N II 916 Å significantly weaker than the N II 1085 Å line (see Table 4). This is expected because the N II 916 Å multiplet is subject to extinction by N_2 bands. We estimate that at 150 km altitude most of the multiplet fine structure is removed by absorption in the N_2 $o_3(2, 0)$, $b'(8, 0)$, and $b(11, 0)$ bands, at $T = 650$ K. The extinction effects therefore aggravate the problem of explaining the strength of this multiplet.

Given these considerations, it is our view that at this juncture a firm conclusion cannot be drawn in respect to the identification of the major source process. The strong morphological effects related to magnetic latitude of both O II 834 Å and N II 1085 Å features above 600 km described by Chakrabarti et al. (1983), suggest that relationships to solar flux input are not simple.

5.4. *Titan Dayglow*

The EUV spectrum of Titan and the Earth airglow contain basic similarities in nitrogen emission features. The Titan spectrum contains relatively stronger N_2 c'_4–X bands, but this can be plausibly explained by differences in abundances of foreground gas; the Titan atmospheric emission is produced mainly in the vicinity of the exobase (Strobel & Shemansky 1982; Conway 1983). Table 4 shows a comparison of relative emission rates obtained from *Voyager 1* UVS observations of Titan to Earth airglow measurements. The table also contains relative strengths for (R1) and (R2). It appears that the planetary data could be satisfactorily reproduced by (R1) with an electron temperature of $T_e \sim 4 \times 10^5$ K. The relationship between N II 670 Å and 747 Å emissions in the Titan spectrum suggests that a substantial contribution from (R3) is not present, indicating a high loss rate for atomic nitrogen produced in the atmosphere by the various dissociative branches. Thus the relative rates of the N II lines at 1085 Å, 916 Å, and 670 Å as derived from the *Voyager* data by Strobel and Shemansky (1982) are compatible with reaction (R1). The contribution of (R4) to N II 1085 Å emission at Titan can be obtained using the same parameters discussed above. Using a deposition level of 10^{17} cm^{-2} in N_2 abundance for the 303.8 Å source line, the combined extinction in CH_4 for 303.8 Å and 1085 Å emission is estimated to be 0.68 at the top of the atmosphere. This provides a calculated contribution of 3 R due to reaction (R4) to the observed total of 12 R in the N II 1085 Å line, using the solar source flux quoted above. The contributions to the N II 916 Å and 670 Å line due to (R4) are negligible.

6. SUMMARY

Laboratory measurements of EUV emission from electron excited N_2 have been obtained at medium resolution, providing N II EUV emission cross section measurements and allowing the confirmation of recent calculations by Fawcett (1987) indicating the presence of a strong intercombination line in N II at 748.37 Å. The most recently available data have been used to predict the basic collisional and radiative properties of N II. We have briefly explored plasma diagnostic properties and provide radiative cooling coefficients. The accuracy of the near threshold collision strengths of a number of transitions that have not been obtained by close coupling calculations is expected to be poor because of strong mixing of states.

Some basic properties of electron excited N II and N_2 have been examined in the EUV for the purpose of diagnosis of emission spectra of the Earth and Titan. The N II emissions in the Earth dayglow particularly at 916 Å are much brighter than current estimates of source rates, particularly in view of significant extinction by N_2. The N II 1085 Å line in the Earth dayglow contains a significant component from dissociative photoionization-excitation, but it is not clear that the emission strength of the line has been explained. Direct measurements of dissociative photoionization-excitation efficiencies are needed to provide definitive rates. If the reaction (R1) plays a significant role in the Earth dayglow, the effective electron temperature must be higher than the value for the predicted photoelectron spectrum. Morphological effects in the Earth airglow described by Chakrabarti et al. (1983) suggest a rather complicated relationship to solar flux input. The N II 1085 Å, 916 Å, and 670 Å lines in the Titan dayglow spectrum appear to be basically compatible with direct electron excitation of N_2. Our examination of these issues is not detailed, and further work with accurate modeling using the more recent nitrogen parameters is in order.

We thank D. T. Hall for many helpful discussions. This work is supported by National Science Foundation grant ATM-8715709, and NASA grants NAGW-649 and NAGW-1904 to the University of Arizona.

APPENDIX A

PHOTOIONIZATION EFFICIENCIES FOR REACTION (R4)

No direct measurements of N II emissions through reaction (R4) of interest here have been published. However, an estimate of the cross sections can be obtained indirectly from a combination of electron and photon excitation measurements. The cross section for the production of the N_2^+ B state in (R4) has been measured by Lee (1977), and the total N_2^+ and N II photon cross sections (1.17×10^{-17} cm^2 at 303.8 Å) have been obtained by Sampson et al. (1987, and references therein). The electron cross sections (R1) for the N_2^+ B and N II states have also been obtained (Borst & Zipf 1970, and references therein; Ajello et al. 1989, and references therein). The electron cross sections can be related to the oscillator strengths through reduction processes such as that described by Shemansky et al. (1985) or by simply establishing the ratio of cross sections at sufficiently high energy so that the first Born term is dominant. On the basis of the directly measured cross sections the yield of the N_2^+ B state from (R4) is $Y(N_2^+ B) = 0.11$ at 303.8 Å. On the basis of electron cross sections the relative yield is $Y(\text{N II } 1085 \text{ Å})/Y(N_2^+ B) = 0.13$. The yield of the N II 1085 Å transition is then $Y(\text{N II } 1085 \text{ Å}) = 0.015$ at 303.8 Å. Similarly we obtain $Y(\text{N II } 916 \text{ Å}) = 0.003$.

REFERENCES

Ajello, J. M., James, G. K., Franklin, B. O., & Shemansky, D. E. 1989, PhyRv., 40, 3524
Ajello, J. M., et al. 1988, AOpt, 27, 890
Bashkin, S., & Stoner, J. R. 1975, Atomic Energy Levels and Grotrian Diagrams (Amsterdam: North-Holland)
Bates, D. R., & Damgaard, A. 1949, PTRSL, 242, 101
Berry, H. G., Bickel, W. S., Bashkin, S., Desesquelles, J., & Schectman, R. M. 1971, JOSA, 61, 947
Blair, W. P., & Raymond, J. C. 1984, BAAS, 15, 930
Borst, W. L., & Zipf, E. C. 1970, PhyRvA, 1, 834
Buchet, J. P., Poulizac, M. C., & Carre, M. 1972, JOSA, 62, 623
Chakrabarti, S. 1986, JGR, 91, 8065
Chakrabarti, S., Paresce, F., Bowyer, S., Kimble, R., & Kumar, S. 1983, JGR, 88, 4898
Chang, M. W. 1977, ApJ, 211, 300
Christensen, A. B. 1976, GRL, 3, 221
Conway, R. R. 1983, JGR, 88, 4784
Cowan, R., Hobbs, L., & York, D. 1982, ApJ, 257, 373
Cox, D. P., & Daltabuit, E. 1971, ApJ, 167, 113
Cox, D. P., & Tucker, W. H. 1969, ApJ, 157, 1157
Czyzak, S. J., & Poirier, C. P. 1985, ApSpSc, 116, 21
Dalgarno, A., & McCray, R. A. 1972, ARAA, 10, 375
Dumont, P. D., Baudinet-Robinet, Y., & Livingston, A. E. 1976, PhyScr, 13, 365
Dumont, P. D., Biemont, E., & Grevesse, N. 1974, JQSRT, 14, 1127
Eastes, R. W., Feldman, P. D., Gentieu, E. P., & Christensen, A. B. 1985, JGR, 90, 6594
Eriksson, K. B. S. 1983, PhyScr, 28, 593
Fawcett, B. C. 1987, Atomic Data Nucl. Data, 37, 411 (F87)
Feldman, P. D., Anderson, D. E., Meier, R. R., & Gentieu, E. P. 1981, JGR, 86, 3583
Ferland, G. J., & Rees, M. J. 1988, ApJ, 332, 141
Gentieu, E. P., Eastes, R. W., Feldman, P. D., & Christensen, A. B. 1989, CanJP, 67, 82
Gentieu, E. P., Feldman, P. D., Eastes, R. W., & Christensen, A. B. 1981, GRL, 8, 1242
———. 1984, JGR, 89, 11053
Gentieu, E. P., Feldman, P. D., & Meier, R. R. 1979, GLR, 6, 325
Goldbach, C., Martin, M., & Nollez, G. 1989, A&A 221, 155
Heroux, L. 1967, PhyRv, 153, 156
Hibbert, A., & Bates, D. R. 1981, PlSpSc, 29, 263
Huber, K. P., & Herzberg, G. 1979 Molecular Spectra and Molecular Structure. IV. Constants of Diatomic Molecules (New York: Van Nostrand Reinhold)
Jackson, A. R. G. 1973, MNRAS, 165, 53
James, G. K., Ajello, J. M., Franklin, B., & Shemansky, D. E. 1990, JPB, in press
Jordan, C. 1969, MNRAS, 142, 501
Kernahan, J. A., Livingston, A. E., & Pinnington, E. H. 1974, CanJC, 52, 1985
Knight, R. D. 1982, PhyRvL 48, 792
Lee, L. C. 1977, JPB, 10, 3033
Livingston, A. E., Baudinet-Robinet, Y., & Dumont, P. D. 1975, PhyRvL, 55, 207
Meier, R. R., Conway, R. R., Feldman, P. D., Strickland, D. J., & Gentieu, E. P. 1982, JGR, 87, 2444
Morrison, M. D., Bowers, C. W., Feldman, P. D., & Meier, R. R. 1990, JGR, 95, 4113
Morrison, M. D., Cunningham, A. J., & Christensen, A. B. 1983, JQSRT, 29, 137
Nussbaumer, H., & Rusca, C. 1979, A&A, 72, 129
Osterbrock, D. E. 1989, Astrophysics of Gaseous Nebulae and Active Galactic Nuclei (Mill Valley, CA: University Science Books)
Park, H., Feldman, P. D., & Fastie, W. G. 1977, GRL, 4, 41
Raymond, J. C. 1988, in Hot Thin Plasmas in Astrophysics, ed. R. Pallavicini (Dordrecht: Kluwer Academic), 3.
Raymond, J. C., Cox, D. P., & Smith, B. W. 1976, ApJ, 204, 290
Robb, W. D. 1975, JPB, 8, L46
Samson, J. A. R., Masuoka, T., Pareek, P. N., & Angel, G. C. 1987, JCP, 86, 6128
Saraph, H. E., Seaton, M. J. 1974, JPB, 7, L36
Seaton, M. J. 1975, MNRAS, 170, 475
Shapiro, P. R., & Moore, R. T. 1976, ApJ, 207, 460
Shemansky, D. E., Ajello, J. M., Hall, D. T., & Franklin, B. 1985, ApJ, 296, 774
Shemansky, D. E., & Smith, G. R. 1981, JGR, 86, 9179
Smith, H., Bromander, J., Curtis, L. J., & Buchta, R. 1970, PhyScr, 2, 211
Strobel, D. F., & Shemansky, D. E. 1982, JGR, 87, 1361
Tarter, C. B. 1977, JQSRT, 17, 531
Trajmar, S., & Register, D. 1984, Electron-Molecule Collisions, ed. I. Shimamura and K. Takayanagi (New York: Plenum Press), p. 427
Wiese, W. L., & Martin, G. A. 1980, Wavelengths and Transition Probabilities for Atoms and Atomic Ions (Washington, DC: US Dept. of Commerce)
Wiese, W. L., Smith, M. W., & Glennon, B. M. 1966, Atomic Transition Probabilities, Vol. I (Washington, DC: US Dept. of Commerce)